NANO LETTERS

Letter

Cite This: Nano Lett. XXXX, XXX, XXX−XXX

pubs.acs.org/NanoLett

Determining GaN Nanowire Polarity and its Influence on Light Emission in the Scanning Electron Microscope

G. Naresh-Kumar,*[,†,∥] J. Bruckbauer,[†,∥] A. Winkelmann,[†,‡,∥] X. Yu,[§] B. Hourahine,[†] P. R. Edwards,[†] T. Wang,[§] C. Trager-Cowan,[†] and R. W. Martin[†]

[†]Department of Physics, SUPA, University of Strathclyde, Glasgow G4 0NG, U.K.

[‡]Laser Zentrum Hannover e.V., 30419 Hannover, Germany

[§]Department of Electronic and Electrical Engineering, University of Sheffield, Sheffield S1 3JD, U.K.

Supporting Information

ABSTRACT: The crystal polarity of noncentrosymmetric wurtzite GaN nanowires is determined nondestructively in the scanning electron microscope using electron backscatter diffraction (EBSD). The impact of the nanowire polarity on light emission is then investigated using cathodoluminescence (CL) spectroscopy. EBSD can determine polarity of noncentrosymmetric crystals by interrogating differences in the intensity distribution of bands of the EBSD pattern associated with semipolar planes. Experimental EBSD patterns from an array of GaN nanowires are compared with theoretical patterns produced using dynamical electron simulations to reveal whether they are Ga- or N-polar or, as in several cases, of mixed polarity. CL spectroscopy demonstrates the effect of the polarity on light emission, with spectra obtained from nanowires of known polarity revealing a small but measurable shift (≈28 meV) in the GaN near band edge emission energy between those with Ga and N polarity. We attributed this energy shift to a difference in impurity incorporation in nanowires of different crystal polarity. This approach can be employed to nondestructively identify polarity in a wide range of noncentrosymmetric nanoscale material systems and provide direct comparison with their luminescence.

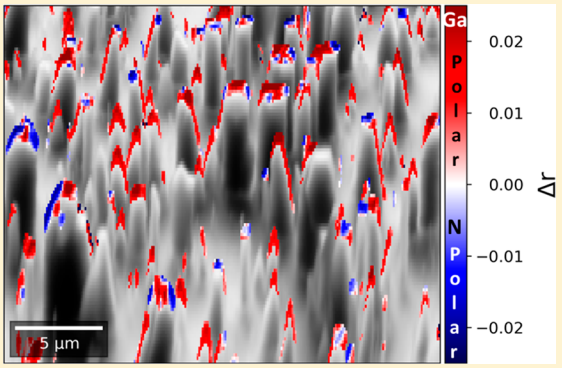

KEYWORDS: *Nanowires, polarity, electron diffraction, SEM, GaN, cathodoluminescence*

The polarity of a crystal surface plays a crucial role in determining many of its physical properties and can also influence the nucleation of subsequent growth on those surfaces. For example in the growth of GaN, the N-polar $(000\bar{1})$ surface is less stable and decomposes more easily than the Ga-polar (0001) surface.[1] The effect of crystal polarity in wurtzite semiconductors (in particular III-nitrides) is highly influential in determining the electrical and optical properties of these material systems.[2−6] One-dimensional structures such as GaN nanowires are highly sought after as building blocks for applications in nanophotonics and electronics for their defect free, large surface area and quantum confinement effects.[2] The lack of inversion symmetry along the *c*-axis of the wurtzite GaN structure causes different polarization induced electric fields for N- and Ga-polar surfaces. While the majority of GaN structures have Ga-polar surfaces,[7] N-polar surfaces offer a great advantage for high electron mobility transistors providing a strong back barrier layer, low resistivity Ohmic contacts and improved capability for large scale device processing.[6] Recently there has been immense interest in determining polarity in semiconductor based nanowires in order to better understand their polarity dependent growth mechanisms.[8−10] In some cases the polarity also determines the final shape of the nanowires and can also be engineered to form new nanostructures.[11]

A range of methods have been used to determine the polarity in GaN nanowires and nanostructures. A number of these are based on transmission electron microscopy (TEM), including convergent beam electron diffraction (CBED)[12] and annular bright field atomic imaging in the aberration corrected scanning TEM.[8] While excellent for characterizing individual nanowires, they require complex sample preparation and usually fail to sample a statistically significant number of nanowires. Selective etching in KOH, or other solvents, has been shown to identify polarity of GaN nanostructures,[13,14] but is by definition destructive. Qualitative analysis based on shape and surface morphology is possible,[13,14] but the presence of inversion domains will complicate morphology based polarity identification.[15,16] Atomic force microscope techniques, such as Kelvin probe force microscopy (KPFM) and piezo force microscopy (PFM) have been used in impressive nondestructive polarity determination in arrays of GaN

Received: March 13, 2019
Revised: April 9, 2019
Published: April 30, 2019

DOI: 10.1021/acs.nanolett.9b01054
Nano Lett. XXXX, XXX, XXX−XXX

nanowires.[3,17,18] The sharp changes in topography present some challenges and, while clear differences in contact potential differences are observed for opposite polarities, the absolute values are found to vary depending on the surface and tip condition. Another elegant method to nondestructively determine GaN nanowire polarity involved the use of coherent X-ray Bragg imaging,[19] although this involves access to a synchrotron. There are benefits in identifying a nondestructive, large-area method for nanowire polarity determination using scanning electron microscopy (SEM). This is the subject of this Letter, which employs electron backscatter diffraction (EBSD) imaging in a field emission scanning electron microscope, providing the opportunity to then deploy complementary imaging techniques such as cathodoluminescence (CL). We have exploited the intensity variations in EBSD patterns due to the breaking of inversion symmetry to image polarity differences in GaN nanowires. We then go on to use coincident CL imaging to demonstrate differences in the emission spectra between nanowires of different polarity.

In EBSD, the sample is tilted at around 70° to the normal of the incident electron beam. The impinging electrons are scattered inelastically through high angles forming a diverging source of electrons which can be diffracted. The resultant electron backscatter diffraction pattern consists of a large number of overlapping bands, known as Kikuchi bands, which correspond to a 2-D projection of the lattice planes in a crystal structure. EBSD is a well-established technique for texture analysis and for quantifying grain boundaries and crystal phases.[20] The introduction of cross-correlation based analysis of EBSD patterns has also made possible measurements on relative strain, geometrically necessary dislocations, and lattice tilt and twist as well as crystal polarity.[21,22] Once the polarity is known, its influence on other material properties, such as light emission, can be assessed. CL hyperspectral imaging[23−25] is an ideal technique with which to investigate light emission from small structures such as nanowires. CL spectroscopy is a widely used technique for optical characterization of light emitting materials and can also provide information on defects, doping and strain.

Here we report coincident EBSD and CL results obtained from self-induced GaN nanowires. The GaN nanowires were grown on 2 in. planar (111) Si substrates in a commercial 3 × 2 in. Thomas Swan close-coupled showerhead reactor using metal organic vapor phase epitaxy. Trimethylaluminum (TMAl), trimethylgallium (TMGa), and ammonia (NH_3) are employed as precursors with H_2 used as the carrier gas for each. Initially, the Si substrate is annealed in a H_2 ambient at 1110 °C for 600 s to remove the natural oxide layer on the surface. Then, 2.7 μmol/min of TMAl is flowed at 1145 °C for 72 s. Preflowing TMAl on the Si substrate generates Al or Al−Si alloy nanodots, which serve as nucleation sites for subsequent GaN nanowire growth performed at 866 °C with 6.2 μmol/min of TMGa and 20 mmol/min of NH_3 for 3800 s. The pressures used during the flow of TMAl and the GaN nanowire growth are 65 and 300 Torr, respectively.

Figure 1 schematically depicts the experimental arrangement used for the coincident EBSD and CL imaging of nanowires. Due to different optimum detector geometries and electron beam energies for the two techniques, we performed CL imaging followed by EBSD imaging. The sample was tilted at 45° toward the light collection optics for CL measurements[25] and at 70° toward the EBSD detector to obtain EBSD maps.[21] Both the EBSD and CL measurements were performed in a

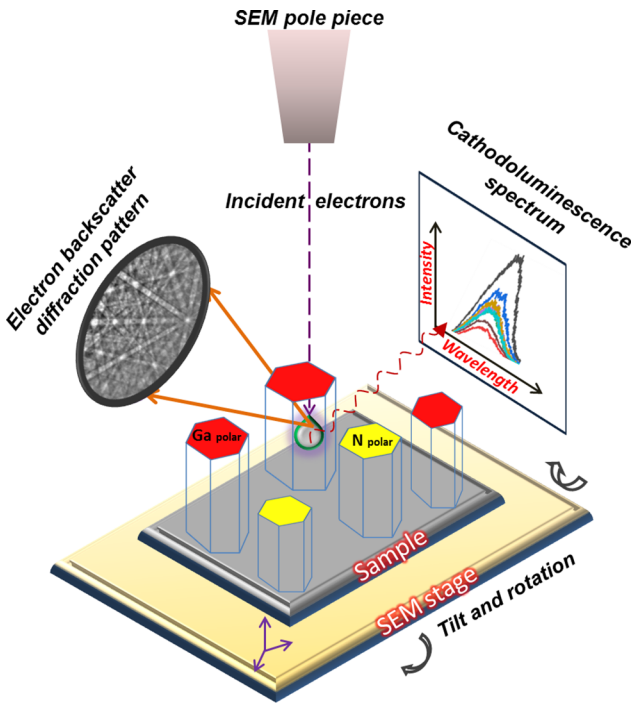

Figure 1. Schematic of the experimental arrangement for coincident EBSD and CL imaging. The SEM stage can be tilted and rotated with the sample normally tilted to 70° for the EBSD and to 45° for the CL, with respect to the normal to the incident electron beam.

variable pressure field emission scanning electron microscope (FEI Quanta 250). The EBSD patterns were obtained using a Nordlys EBSD detector from Oxford Instruments with electron beam energy of 20 keV and a probe current of ∼2 nA. By moving a focused electron beam point by point across a grid of positions on the surface of the nanowires, the EBSD maps were recorded by acquiring an EBSD pattern for every 100 nm with a pattern resolution of 672 × 512 pixels with 350 ms acquisition time. CL is performed in hyperspectral imaging mode using a custom-built CL system attached to the SEM, where a spectrally resolved luminescence spectrum is collected for every pixel in the image with a spatial resolution approaching 10 nm.[24,25] The light was collected by a Cassegrain reflecting objective, dispersed with a 1/8 m focal length spectrometer (Oriel MS125) and collected using a 1600-channel electron multiplying charge-coupled device (Andor Newton). The CL data set was recorded at room temperature with an electron beam energy of 5 keV and a probe current in the range of 100s of pA.

The secondary electron (SE) images in Figure 2a,b illustrate that the growth method used gives rise to nanowires with a range of diameters (≈50−2000 nm). A typical EBSD pattern acquired from a GaN nanowire is shown in Figure 2c. To a first approximation, the visible bands in an EBSD pattern can be interpreted as the projection of lattice planes (hkl) relative to point source emitters inside the crystal. The Kikuchi bandwidth is approximately twice the Bragg angle between the two band edges, which are the result of the reflections (hkl) and ($\bar{h}\ \bar{k}\ \bar{l}$), respectively. For a quantitative simulation of the intensity distributions in EBSD patterns, the strong effects of multiple scattering and absorption of backscattered electrons need to be considered, and hence dynamical theory of electron diffraction[26] becomes mandatory. While detailed reviews on various models for EBSD pattern simulations and the physics

DOI: 10.1021/acs.nanolett.9b01054
Nano Lett. XXXX, XXX, XXX−XXX

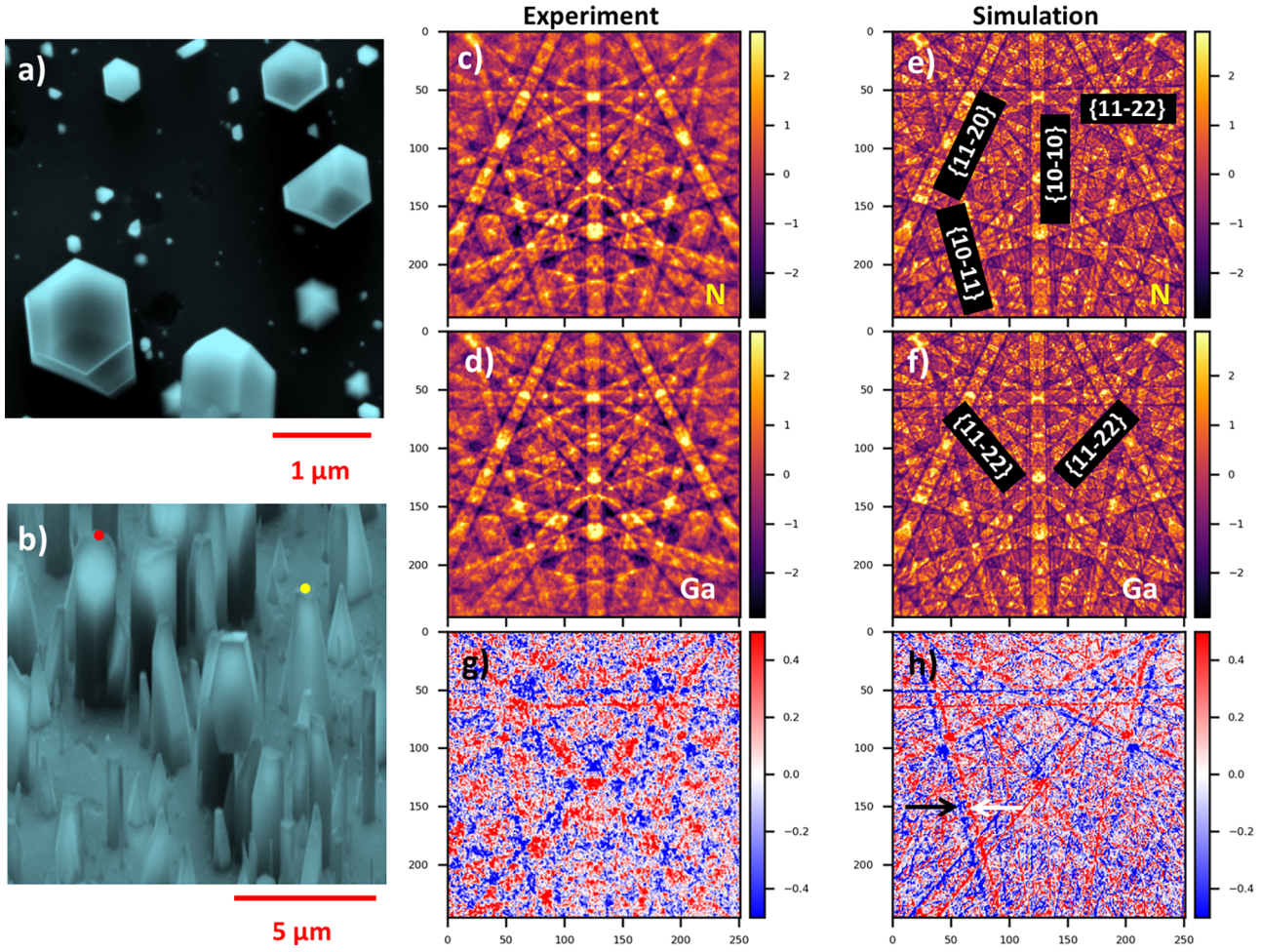

Figure 2. (a) Plan view SE image (top down view), (b) SE image acquired by tilting the sample to 70°, (c) experimental EBSD pattern from the solid yellow circle area, (d) experimental EBSD pattern from the solid red circle area, (e, f) simulated patterns for N and Ga polarity, respectively, (g) normalized intensity difference image of experimental EBSD patterns (from (c) and (d)), and (h) normalized intensity difference image of simulated EBSD patterns (from (e) and (f)). The white arrow points to $\{10\bar{1}1\}$ and the black arrow points to $\{10\bar{1}\,\bar{1}\}$.

underpinning EBSD pattern formation can be found elsewhere,[26,27] a main outcome of dynamical electron scattering is a pronounced sensitivity of EBSD patterns to the possible absence of a center of inversion in a crystal structure.[28] This is why the quantitative analysis of EBSD patterns via realistic electron diffraction simulation can deliver considerable additional information beyond the geometrical positions of the Kikuchi bands. In the noncentrosymmetric wurtzite structure of GaN, for example, the inequivalence of the Bragg reflections on either side of certain Kikuchi bands leads to an asymmetric band profile, with the intensity maximum slightly shifted from the center of these Kikuchi bands.[29] A comparison with simulated patterns makes it possible to assign the correct (hkl) and $(\bar{h}\,\bar{k}\,\bar{l})$ to the Kikuchi band edges and thus to determine the positive direction of the polar c-axis in the GaN nanostructure.

We note that a different, and less informative, intensity asymmetry in Kikuchi bands can arise due to the so-called "excess-deficiency effects",[30] which are the result of the experimental scattering geometry with strong forward peaked differential scattering cross sections. The quantitative development of Kikuchi band asymmetries via excess-deficiency effects depends on the relative orientation of the respective Kikuchi bands with respect to the incident beam direction and can be minimized by careful selection of the sample orientation.

To determine the crystal polarity, the EBSD patterns of the GaN nanowires have been analyzed using the method described in ref 29. In summary, on the basis of a starting orientation identified by the EBSD manufacturer's software, we first look for an optimized crystal orientation by maximizing the normalized cross-correlation coefficient r (ref 31) between the experimental pattern and simulated data (see Supporting Information S1 for more details). The experimental EBSD patterns were analyzed using the Bloch wave approach for calculating the simulated EBSD patterns according to ref 26. For the dynamical Kikuchi pattern simulations of the GaN crystal structure, we took into account a set of 2340 reciprocal lattice vectors with a minimum lattice spacing $d_{hkl} > 0.035$ nm. For interpreting the EBSD patterns, the crystal orientations were parametrized using the ZXZ-type Euler angles ($\phi 1$, φ, $\phi 2$) in the Bunge convention.[20] As the manufacturer orientations do not account for noncentrosymmetric structures, we then explicitly test for a possible better fit of the inverted GaN crystal structure. This is equivalent to the effect of a 2-fold rotation of the simulated data perpendicular to the polar c-axis direction.[22] This makes it possible to absolutely determine the positive direction of the c-axis along the

DOI: 10.1021/acs.nanolett.9b01054
Nano Lett. XXXX, XXX, XXX−XXX

nanowire, i.e., whether [0001] ("Ga polarity") or [000$\bar{1}$] ("N polarity"). Parts c and d of Figure 2 show the experimental EBSD patterns recorded from regions of nanowires marked with solid yellow and red circles in Figure 2b, respectively. The patterns have been normalized by subtracting the mean and dividing by the standard deviation, such that the intensity scales show the deviation from the mean intensity in terms of the standard deviation and provide comparable contrast and brightness scales. The simulated patterns for N polarity and Ga polarity are shown in Figure 2e,f, respectively. A quantitative comparison of the experimental EBSD pattern shown in Figure 2c with the simulated patterns gives different r values of 0.73 and 0.71 in the test for N polarity and Ga polarity, respectively. The difference of Δr = 0.02 is sufficient to indicate a significantly better fit of the N polar orientation relative to the Ga polarity.[22,29] The same approach was repeated for the experimental EBSD pattern shown in Figure 2d, which resulted in a better fit with r = 0.74 for the Ga polarity as compared to r = 0.72 for the N polarity.

At first sight, both the experimental (Figure 2c,d) and the simulated EBSD patterns (Figure 2e,f) look extremely similar. Careful inspection reveals differences in the intensity of some Kikuchi bands, especially along the {10$\bar{1}$1} bands where the higher intensity is toward either the top or bottom of the respective Kikuchi band edge. This can also be seen clearly in the difference images between the two experimental EBSD patterns and the corresponding simulated patterns as shown in Figure 2g,h, respectively. In order to aid the comparison of the expected theoretical and the observed intensity differences seen in Figure 2g,h (where the greatest differences in intensity manifest as "lines" of blue and red), we have indicated in Figure 3 which Kikuchi bands will be affected by polarity

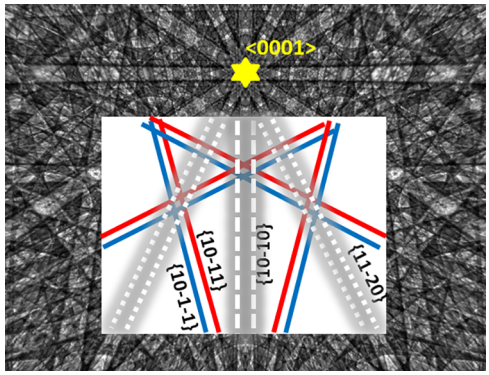

Figure 3. Indication of the expected intensity differences in Kikuchi bands resulting from lattice planes that are sensitive to the absence of a center of inversion in the GaN structure. Red (blue) corresponds to a positive (negative) intensity difference, as in Figure 2. The gray bands are insensitive to polarity effects because they correspond to lattice planes that contain the polar c-axis (i.e., these bands cross at the ⟨0001⟩ zone axes, marked with a yellow star).

effects with red and blue lines and which bands are insensitive to the absence of a center of symmetry (gray bands). The schematic of Figure 3 shows that the red and blue regions in Figure 2g,h are consistent with the assumption that the experimental pattern in Figure 2c belongs to an N-polar nanowire, while the pattern in Figure 2d is from a Ga-polar nanowire.

The observed intensity differences in Kikuchi bands from {10$\bar{1}$1} and {10$\bar{1}\bar{1}$} lattice planes clearly indicate the breaking of inversion symmetry and confirm the different polarities seen in the GaN nanowires. In particular noncentrosymmetric {10$\bar{1}$1} lattice planes in GaN provide the largest Kikuchi band asymmetries due to breaking of inversion symmetry. The Kikuchi bands corresponding to these planes were deliberately acquired diagonally (see Figure 2) with respect to the detector to reduce the contribution from parasitic excess-deficiency effects which are unrelated to polarity. The strength of the excess-deficiency asymmetry depends on the orientation of the respective lattice plane relative to the incident beam direction. Kikuchi bands associated with lattice planes whose normal is directed perpendicular to the tilting axis of the sample, are most affected in the EBSD geometry.[32] On the detection screen, these bands are thus oriented nearly horizontally, as for example the {11$\bar{2}$2} band seen in Figure 2e. For the orientation of our sample, the intensity asymmetry in the horizontal {11$\bar{2}$2} band is visibly influenced by the excess-deficiency effect. We have checked that the relative effect on the pattern near the horizontal {11$\bar{2}$2} band is still sufficiently small as not to lead to an erroneous assignment of the opposite polarity for the full pattern. Our full-pattern matching approach, involving a number of different noncentrosymmetric bands in a large solid angle, is very stable against the excess-deficiency effect, because the polarity asymmetries need to be fitted consistently in all observed bands. In comparison, for a single Kikuchi band, the reliable discrimination of a polarity asymmetry is only possible when this asymmetry is larger than the local influence of excess-deficiency effect. With respect to the different sensitivity of specific Kikuchi bands to polarity effects, we can also notice the disappearance of Kikuchi bands corresponding to {11$\bar{2}$0} and {10$\bar{1}$0} nonpolar planes in the difference images (see Figure 2h and in Figure 3 represented as shaded gray bands). The lattice plane normals corresponding to these Kikuchi bands are perpendicular to the c-axis which has 6-fold symmetry.[33] When a lattice plane contains an even-fold rotation axis, we cannot discriminate between the (hkl) and $(\bar{h}\,\bar{k}\,\bar{l})$ directions pointing along the opposite directions of the plane.[29]

To identify nanowires with different polarity, we have also acquired an EBSD map covering a range of nanowires of various dimensions. Figure 4a shows a backscattered electron (BSE) image acquired using the solid state BSE detector, which is positioned underneath the EBSD detector. The EBSD detector can also act as an imaging device, in this case treating the whole EBSD detector as a virtual diode. This is shown in Figure 4b, where the BSE intensity image was derived from the complete raw EBSD patterns (gray color image) at each pixel in the resultant map. In Figure 4b, we also show the resulting change Δr of the cross-correlation coefficient relative to the simulation for the [0001] Ga-polar orientation; i.e., positive/negative values of Δr indicate a better fit of the Ga polarity (red) or the N polarity (blue), respectively. In order to exclude the low-quality patterns for which the polarity discrimination is unreliable due to shadowing effects by the extreme nanowire topography, the data points shown in Figure 4b have been limited to patterns with $r > 0.3$ with respect to the simulation. After this thresholding, the colored regions indicate the observation of Kikuchi patterns where there are significant changes in r of the order of $|\Delta r| > 0.01$,[29] when compared to both possible orientations. Most of the nanowires are observed to be predominantly Ga-polar; however, there are a number of nanowires with both polarities present. A number of the nanowires exhibit top facets that are nitrogen polarity with side

DOI: 10.1021/acs.nanolett.9b01054
Nano Lett. XXXX, XXX, XXX−XXX

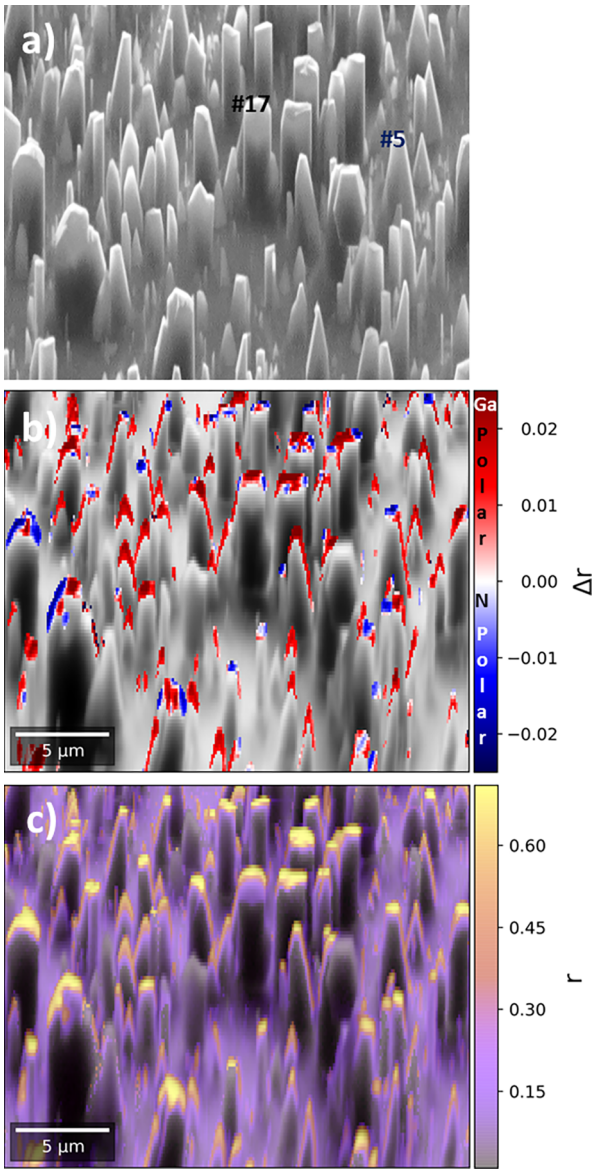

Figure 4. (a) Backscatter electron (BSE) image acquired using a solid state BSE detector, numbers #5 and #17 correspond to regions where CL spectra were extracted from the hyperspectral data set (see Figure 5), (b) cross-correlation difference map showing Ga oriented wires in red and N oriented wires in blue, overlaid on a BSE intensity image derived from the raw EBSD patterns, and (c) cross-correlation map showing that the largest values arise from the top region of the nanowires. Note that some nanowires show both crystal polarities.

facets that are Ga polarity. Note that the best values for the cross-correlation coefficient are obtained from the top region of the nanowires (see Figure 4c).

As the Si substrate is nonpolar, resultant growth of AlN or GaN can be of either polarity, and mixed polarity nanowires are also observed.[16−18,34,35] The nanowires with mixed polarity will contain inversion domain boundaries (IDB) separating domains of Ga and N polarity as reported in refs 19 and 36. Inversion domains have been reported to originate from eutectic Al−Si reactions for Si (111) substrates.[17] As our nanowires are likely to have nucleated from Al−Si alloy nanodots, it is perhaps not surprising that our nanowires exhibit mixed polarities. Chemical etching using a KOH solution showed regions of N-polar nanowires affected by the etchant and some nanowires also show other crystal facets in addition to the predominant *c*-plane (see Supporting Information S2).

CL imaging was performed on the same area of nanowires as the previous EBSD measurement, as shown in Figure 4b, allowing the investigation of the optical properties of the different polarity regions identified by EBSD. Figure S3 in the Supporting Information shows the area for coincident CL and EBSD imaging with selected nanowires marked by numbers. Due to the light collection geometry, only the top surfaces of the nanowires were facing the collection optics. Light excited at the side of the nanowires has to pass through the nanowires before reaching the collection optics, which leads to self-absorption and artificial shifts in energy. For this reason only spectra excited at the top surface facing the collection optics were considered and were extracted from the hyperspectral data set.[37] The spectra are then plotted according to the polarity identification from the EBSD maps, as shown in Figure 4b. Parts a and b of Figure 5 show the CL spectra of the GaN near band edge (NBE) emission for several Ga-polar and N-polar nanowires, respectively, normalized to the NBE peak height and offset vertically for clarity. Nanowires #5 and #17 correspond to the solid yellow circle region (N-polar) and red circle region (Ga-polar), respectively (see Figure 2b). Nanowires #5, #6, and #11 exhibit both polarities as shown in the NBE spectra acquired from Ga-polar and N-polar regions of the same nanowire (see Figure 5a,b). The Ga-polar nanowires exhibit a GaN NBE emission centered predominantly around 368 nm (≈3.37 eV), whereas the N-polar nanowires show a blue-shifted emission peak around 365 nm (≈3.40 eV). As a guide for the eye the vertical dashed lines in Figure 5a,b represent the approximate peak position of the Ga-polar nanowires.

Several causes could lead to this observed ≈3 nm (28 meV) shift in emission wavelength (energy). First, the nanowires could undergo strain relaxation during the growth. However, if this were the case, there should be a distribution of peak energies since the nanowires exhibit varying dimensions, as seen in Figure 2a,b. A more likely strain-related possibility is that there has been a relative change in the overall strain within the nanowire due to the change in growth mode for the different polarities, which would lead to two distinct energies. Furthermore, the emission energy can also be influenced by quantum confinement caused by the different diameters of the nanowires.[38] This can be excluded because the different sizes of the nanowires should again lead to a spread of energies. A more likely possibility is that this observed shift in energy is related to different levels of unintentional doping in the nanowires of different polarities, for which Si- and O-doping are possible candidates.[39,40] Si is a common n-type dopant in GaN and other III-nitrides and is also used as the substrate here. It has been shown for GaN epilayers that the Si-doping concentration is different for Ga and N terminated surfaces, which in turn has an effect on the GaN NBE emission.[39] The Si-doping concentration is generally higher for the N-polar orientation than the Ga-polar one. This leads to a shift of the NBE energy of the N-polar nanowires to higher energies due to the Burstein−Moss effect (band filling).[39] This effect has been seen for wurtzite GaN nanowires where the Si-doping concentration was changed along the nanowire axis and larger contributions from N-polar segments have been observed in the regions of the nanowire with higher Si-doping.[2] A similar shift in CL spectra was observed from the N-polar and Ga-

DOI: 10.1021/acs.nanolett.9b01054
Nano Lett. XXXX, XXX, XXX−XXX

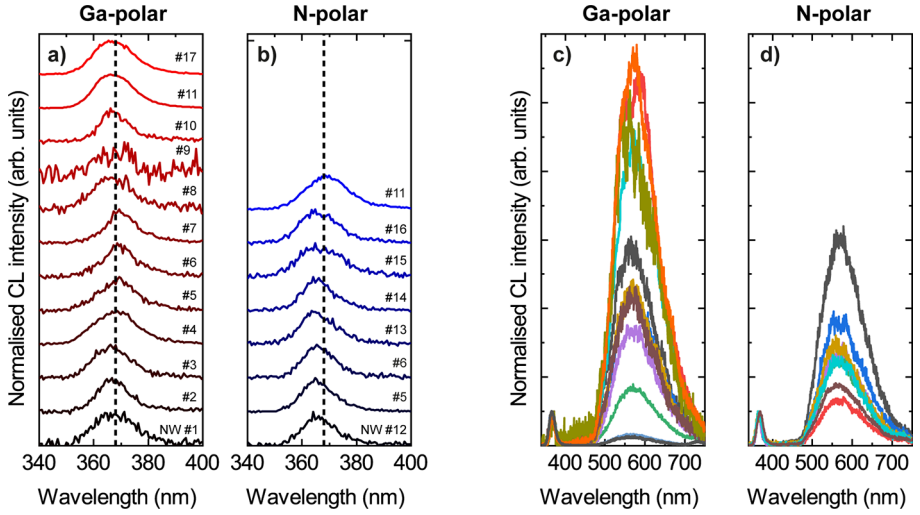

Figure 5. Room temperature CL spectra extracted from a single hyperspectral CL data set, showing the GaN NBE emission for several (a) Ga-polar and (b) N-polar nanowires. The spectra are taken from the top of the nanowires, are normalized to the GaN NBE peak height, and are offset vertically for clarity. The vertical dashed lines show the approximate peak position of the Ga-polar nanowires. (c) and (d) show the same spectra without the offset but for the entire recorded spectral range for the Ga-polar and N-polar nanowires, respectively. The numbers in (a) and (b) refer to selected nanowires shown in Figure S3 in the Supporting Information. Nanowires #5, #6, and #11 exhibit both polarities.

polar regions in GaN polarity junctions in ref 41, but the origin of this shift was not addressed, with photoluminescence measurements in the same reference showing an opposite shift.

Parts c and d of Figure 5 display the same CL spectra as parts a and b of Figure 5 but now normalized to the GaN NBE peak height, without the vertical offset and showing the entire recorded spectral range including the yellow band (YB) emission for Ga-polar and N-polar nanowires, respectively. Comparing the YB emission of the set of Ga-polar and N-polar nanowires, the N-polar nanowires show an overall reduced contribution from the defect-related YB emission. The origin of the yellow band is not unambiguously resolved, but it is related to defect recombination involving a combination of deep or shallow donor and acceptor states (e.g., Ga and N vacancies, interstitials, oxygen, and carbon complexes).[42−44] Literature reports indicate that Si-doping concentrations are generally higher for N-polar structures and that Si-doping decreases the defect density related to the YB emission, leading to a reduction in its intensity.[45] We have observed such a reduced YB emission for the N-polar nanowires compared with the Ga-polar ones, as shown in Figure 5d. This is in agreement with observations from nanowires exhibiting dual polarity.[2,46] Furthermore, this association with Si-doping agrees with the analysis of the shift of the NBE emission as described earlier. Despite these two separate impacts on the nanowires emission properties, there remains too much uncertainty to determine the nanowire polarity using CL imaging alone. However, the use of coincident EBSD and CL imaging provides information on the impact of crystal polarity, and associated changes in impurity incorporation, on light emission.

In summary, we have shown the capability of coincident EBSD-CL imaging in a scanning electron microscope to nondestructively identify crystal polarity in GaN nanowires. The asymmetric intensity distributions within the EBSD patterns from noncentrosymmetric lattice planes due to breaking of inversion symmetry have been exploited to reveal polarity differences in GaN nanowires. The polarity determination was achieved by comparing the experimental EBSD patterns with the simulated patterns incorporating dynamical diffraction effects. CL spectra obtained from the same nanowires reveal a shift in the band edge emission energy between the Ga and N polar nanowires, which we attribute to a difference in impurity incorporation in wires having different crystal polarities. The approach described in our work can be adopted for characterizing a wide range of noncentrosymmetric nanoscale material systems ranging from CdSe quantum dots and nanorods to III−V semiconductor nanostructures such as GaAs/InP and GaN/AlN quantum wells, and nanowires.

■ ASSOCIATED CONTENT

Supporting Information

The Supporting Information is available free of charge on the ACS Publications website at DOI: 10.1021/acs.nanolett.9b01054.

Additional information on polarity verification by etching and the location for correlative EBSD and CL measurements, including secondary electron images and near band edge images (PDF)

■ AUTHOR INFORMATION

Corresponding Author

*E-mail: naresh.gunasekar@strath.ac.uk.

ORCID

G. Naresh-Kumar: 0000-0002-9642-8137
J. Bruckbauer: 0000-0001-9236-9320
B. Hourahine: 0000-0002-7667-7101
P. R. Edwards: 0000-0001-7671-7698
T. Wang: 0000-0001-5976-4994

Author Contributions

‖The manuscript was written through contributions of all authors. All authors have given approval to the final version of the manuscript. G.N-K., J.B., and A.W. have contributed equally.

Notes

The authors declare no competing financial interest.

DOI: 10.1021/acs.nanolett.9b01054
Nano Lett. XXXX, XXX, XXX−XXX

Datasets for the figures in this paper can be found at https://dx.doi.org/10.15129/b152a121-3495-4235-b9cd-985bf1355cd8.

■ ACKNOWLEDGMENTS

This work was supported by the UK EPSRC projects EP/M015181/1, "Manufacturing of nano-engineered III-nitride", EP/P015719/1, "Quantitative non-destructive nanoscale characterisation of advanced materials", and EP/P006973/1, "Future Compound Semiconductor Manufacturing Hub".

■ REFERENCES

(1) Hellman, E. S. The Polarity of GaN: a Critical Review. *MRS Internet J. Nitride Semicond. Res.* **1998**, *3*, E11.
(2) Salomon, D.; Messanvi, A.; Eymery, J.; Martinez-Criado, G. Silane-Induced N-polarity in wires probed by a synchrotron nanobeam. *Nano Lett.* **2017**, *17*, 946−952.
(3) Minj, A.; Cros, A.; Garro, N.; Colchero, J.; Auzelle, T.; Daudin, B. Assessment of Polarity in GaN Self-Assembled Nanowires by Electrical Force Microscopy. *Nano Lett.* **2015**, *15*, 6770−6776.
(4) Akyol, F.; Nath, D. N.; Gur, E.; Park, P. S.; Rajan, S. N-Polar III−Nitride Green (540 nm) Light Emitting Diode. *Jpn. J. Appl. Phys.* **2011**, *50*, 052101.
(5) Chang, J. Y.; Kuo, Y. K. Simulation of N-face InGaN-based p-i-n solar cells. *J. Appl. Phys.* **2012**, *112*, 033109.
(6) Man Hoi Wong et Wong, M. H.; Keller, S.; Dasgupta, N. S.; Denninghoff, D. J.; Kolluri, S.; Brown, D. F.; Lu, J.; Fichtenbaum, N. A.; Ahmadi, E.; Singisetti, U.; Chini, A.; Rajan, S.; DenBaars, S. P.; Speck, J. S.; Mishra, U. K. N-polar GaN epitaxy and high electron mobility transistors. *Semicond. Sci. Technol.* **2013**, *28*, 074009.
(7) Deng, G.; Zhang, Y.; Huang, Z.; Yan, L.; Li, P.; Han, X.; Yu, Y.; Chen, L.; Zhao, D.; Du, G. The growth optimization and mechanism of N-polar GaN films with an in situ porous SiN_x Interlayer. *CrystEngComm* **2017**, *19*, 4330−4337.
(8) de la Mata, M.; Magen, C.; Gazquez, J.; Utama, M. I. B.; Heiss, M.; Lopatin, S.; Furtmayr, F.; Fernandez-Rojas, C. J.; Peng, B.; Morante, J. R.; Rurali, R.; Eickhoff, M.; Morral, A. F. I.; Xiong, Q.; Arbiol, J. Polarity Assignment in ZnTe, GaAs, ZnO, and GaN-AlN Nanowires from Direct Dumbbell Analysis. *Nano Lett.* **2012**, *12*, 2579−2586.
(9) Oppo, C. I.; Malindretos, J.; Zamani, R. R.; Broxtermann, D.; Segura-Ruiz, J.; Martinez-Criado, G.; Ricci, P. C.; Rizzi, A. Polarity dependent strongly inhomogeneous In-incorporation in GaN nanocolumns. *Nanotechnology* **2016**, *27*, 355703.
(10) Li, S. F.; Fuendling, S.; Wang, X.; Merzsch, S.; Al-Suleiman, M. A. M.; Wei, J. D.; Wehmann, H. H.; Waag, A.; Bergbauer, W.; Strassburg, M. Polarity and its influence on growth mechanism during MOVPE growth of GaN sub-micrometer rods. *Cryst. Growth Des.* **2011**, *11*, 1573−1577.
(11) Wang, Z. L. Nanostructures of zinc oxide. *Mater. Today* **2004**, *7*, 26−33.
(12) Roshko, A.; Brubaker, M. D.; Blanchard, P. T.; Bertness, K. A.; Harvey, T. E.; Geiss, R. H.; Levin, I. Comparison of convergent beam electron diffraction and annular bright field atomic imaging. *J. Mater. Res.* **2017**, *32*, 936−946.
(13) Chen, X. J.; Perillat-Merceroz, G.; Sam-Giao, D.; Durand, C.; Eymery, J. Homoepitaxial growth of catalyst-free GaN wires on N-polar substrates. *Appl. Phys. Lett.* **2010**, *97*, 151909.
(14) Bergbauer, W.; Strassburg, M.; Kölper, Ch.; Linder, N.; Roder, C.; Lähnemann, J.; Trampert, A.; Fündling, S.; Li, S. F.; Wehmann, H. H.; Waag, A. Continuous-flux MOVPE growth of position-controlled N-face GaN nanorods and embedded InGaN quantum wells. *Nanotechnology* **2010**, *21*, 305201.
(15) Urban, A.; Malindretos, J.; Klein-Wiele, J.-H.; Simon, P.; Rizzi, A. Ga-polar GaN nanocolumn arrays with semipolar faceted tips. *New J. Phys.* **2013**, *15*, 053045.
(16) Roshko, A.; Brubaker, M.; Blanchard, P.; Harvey, T.; Bertness, K. Selective Area Growth and Structural Characterization of GaN Nanostructures on Si (111) Substrates. *Crystals* **2018**, *8*, 366.
(17) Brubaker, M. D.; Roshko, A.; Blanchard, P. T.; Harvey, T. E.; Sanford, N. A.; Bertness, K. A. Spontaneous growth of GaN nanowire nuclei on N- and Al-polar AlN: A piezo response force microscopy study of crystallographic polarity. *Mater. Sci. Semicond. Process.* **2016**, *55*, 67−71.
(18) Hetzl, M.; Kraut, M.; Hoffmann, T.; Stutzmann, M. Polarity Control of Heteroepitaxial GaN Nanowires on Diamond. *Nano Lett.* **2017**, *17*, 3582−3590.
(19) Labat, S.; Richard, M.; Dupraz, M.; Gailhanou, M.; Beutier, G.; Verdier, M.; Mastropietro, F.; Cornelius, T. W.; Schulli, T. U.; Eymery, J.; Thomas, O. Inversion domain boundaries in GaN wires revealed by coherent Bragg imaging. *ACS Nano* **2015**, *9*, 9210−9216.
(20) Engler, O.; Randle, V. *Introduction to Texture Analysis: Macrotexture, Microtexture, and Orientation Mapping*, second ed.; Taylor and Francis: Boca Raton, FL, 2009.
(21) Vilalta-Clemente, A.; Naresh-Kumar, G.; Nouf-Allehiani, M.; Gamarra, P.; Di Forte-Poisson, M. A.; Trager-Cowan, C.; Wilkinson, A. J. Cross-correlation based high resolution electron backscatter diffraction and electron channelling contrast imaging for strain mapping and dislocation distributions in InAlN thin films. *Acta Mater.* **2017**, *125*, 125−135.
(22) Winkelmann, A.; Nolze, G.; Himmerlich, M.; Lebedev, V.; Reichmann, A. Point-Group Sensitive Orientation Mapping Using EBSD. *Proceedings of the 6th International Conference on Recrystallization and Grain Growth*; Wiley, 2016; pp 281−286.
(23) Christen, J.; Grundmann, M.; Bimberg, D. Scanning cathodoluminescence microscopy: A unique approach to atomic-scale characterization of heterointerfaces and imaging of semiconductor inhomogeneities. *J. Vac. Sci. Technol., B: Microelectron. Process. Phenom.* **1991**, *9*, 2358−2368.
(24) Bruckbauer, J.; Edwards, P. R.; Wang, T.; Martin, R. W. High resolution cathodoluminescence hyperspectral imaging of surface features in InGaN/GaN multiple quantum well structures. *Appl. Phys. Lett.* **2011**, *98*, 141908.
(25) Edwards, P. R.; Jagadamma, L. K.; Bruckbauer, J.; Liu, C.; Shields, P.; Allsopp, D.; Wang, T.; Martin, R. W. High-resolution cathodoluminescence hyperspectral imaging of nitride nanostructures. *Microsc. Microanal.* **2012**, *18*, 1212−1219.
(26) Winkelmann, A.; Trager-Cowan, C.; Sweeney, F.; Day, A. P.; Parbrook, P. J. Many-beam dynamical simulation of electron backscatter diffraction patterns. *Ultramicroscopy* **2007**, *107*, 414−421.
(27) Schwarzer, R. A.; Field, D. P.; Adams, B. L.; Kumar, M.; Schwartz, A. J. *Electron Backscatter Diffraction in Materials Science*; Springer: New York, 2009.
(28) Nolze, G.; Grosse, C.; Winkelmann, A. Kikuchi pattern analysis of noncentrosymmetric crystals. *J. Appl. Crystallogr.* **2015**, *48*, 1405−1419.
(29) Winkelmann, A.; Nolze, G. Point-group sensitive orientation mapping of non-centrosymmetric crystals. *Appl. Phys. Lett.* **2015**, *106*, 072101.
(30) Winkelmann, A. Dynamical effects of anisotropic inelastic scattering in electron backscatter diffraction. *Ultramicroscopy* **2008**, *108*, 1546−1550.
(31) Gonzalez, R. C.; Woods, R. E. *Digital Image Processing*, 2nd ed.; Addison-Wesley Longman Publishing Co., Inc.: Boston, 1992.
(32) Naresh-Kumar, G.; Vilalta-Clemente, A.; Jussila, H.; Winkelmann, A.; Nolze, G.; Vespucci, S.; Nagarajan, S.; Wilkinson, A. J.; Trager-Cowan, C. Quantitative imaging of anti-phase domains by polarity sensitive orientation mapping using electron backscatter diffraction. *Sci. Rep.* **2017**, *7*, 10916.
(33) Gil, B. *Physics of Wurtzite Nitrides and Oxides*; Springer: Switzerland, 2009; pp 1−48.
(34) Brubaker, M. D.; Duff, S. M.; Harvey, T. E.; Blanchard, P. T.; Roshko, A.; Sanders, A. W.; Sanford, N. A.; Bertness, K. A. Polarity-controlled GaN/AlN nucleation layers for selective-area growth of

DOI: 10.1021/acs.nanolett.9b01054
Nano Lett. XXXX, XXX, XXX−XXX

GaN nanowire arrays on Si(111) substrates by molecular beam epitaxy. *Cryst. Growth Des.* **2016**, *16*, 596−604.
(35) Blumberg, C.; Grosse, S.; Weimann, N.; Tegude, F. J.; Prost, W. Polarity-and Site-Controlled Metal Organic Vapor Phase Epitaxy of 3D-GaN on Si (111). *Phys. Status Solidi B* **2018**, *255*, 1700485.
(36) Mkhoyan, K. A.; Batson, P. E.; Cha, J.; Schaff, W. J.; Silcox, J. Direct determination of local lattice polarity in crystals. *Science* **2006**, *312*, 1354.
(37) Bruckbauer, J.; Edwards, P. R.; Bai, J.; Wang, T.; Martin, R. W. Probing light emission from quantum wells within a single nanorod. *Nanotechnology* **2013**, *24*, 365704.
(38) Kim, H. M.; Kim, D. S.; Kim, D. Y.; Kang, T. W.; Cho, Y. H.; Chung, K. S. Growth and characterization of single-crystal GaN nanorods by hydride vapor phase epitaxy. *Appl. Phys. Lett.* **2002**, *81*, 2193−2195.
(39) Prystawko, P.; Leszczynski, M.; Beaumont, B.; Gibart, P.; Frayssinet, E.; Knap, W.; Wisniewski, P.; Bockowski, M.; Suski, T.; Porowski, S. Doping of homoepitaxial GaN layers. *Phys. Status Solidi B* **1998**, *210*, 437−443.
(40) Fichtenbaum, N. A.; Mates, T. E.; Keller, S.; DenBaars, S. P.; Mishra, U. K. Impurity incorporation in heteroepitaxial N-face and Ga-face GaN films grown by metalorganic chemical vapor deposition. *J. Cryst. Growth* **2008**, *310*, 1124−1131.
(41) Kirste, R.; Collazo, R.; Callsen, G.; Wagner, M. R.; Kure, T.; Reparaz, J. S.; Mita, S.; Xie, J.; Rice, A.; Tweedie, J.; Sitar, Z.; Hoffmann, A. Temperature dependent photoluminescence of lateral polarity junctions of metal organic chemical vapor deposition grown GaN. *J. Appl. Phys.* **2011**, *110*, 093503.
(42) Hofmann, D. M.; Kovalev, D.; Steude, G.; Meyer, B. K.; Hoffmann, A.; Eckey, L.; Heitz, R.; Detchprom, T.; Amano, H.; Akasaki, I. Properties of the yellow luminescence in undoped GaN epitaxial layers. *Phys. Rev. B: Condens. Matter Mater. Phys.* **1995**, *52*, 16702−16706.
(43) Neugebauer, J.; De-Walle, C. G. V. Gallium vacancies and the yellow luminescence in GaN. *Appl. Phys. Lett.* **1996**, *69*, 503−505.
(44) Demchenko, D. O.; Diallo, I. C.; Reshchikov, M. A. Yellow Luminescence of Gallium Nitride Generated by Carbon Defect Complexes. *Phys. Rev. Lett.* **2013**, *110*, 087404.
(45) Li, S.; Mo, C.; Wang, L.; Xiong, C.; Peng, X.; Jiang, F.; Deng, Z.; Gong, D. The influence of Si-doping to the growth rate and yellow luminescence of GaN grown by MOCVD. *J. Lumin.* **2001**, *93*, 321−326.
(46) Coulon, P. M.; Mexis, M.; Teisseire, M.; Jublot, M.; Vennegues, P.; Leroux, M.; Zuniga-Perez, J. Dual-polarity GaN micropillars grown by metalorganic vapour phase epitaxy: Cross-correlation between structural and optical properties. *J. Appl. Phys.* **2014**, *115*, 153504.

DOI: 10.1021/acs.nanolett.9b01054
Nano Lett. XXXX, XXX, XXX−XXX